THE ASTROPHYSICAL JOURNAL, 161:541–551, August 1970

A NUMERICAL EXAMPLE OF THE COLLAPSE OF A ROTATING MAGNETIZED STAR*

J. M. LEBLANC AND J. R. WILSON
Lawrence Radiation Laboratory, University of California, Livermore
Received 1969 September 25, revised 1970 January 5

ABSTRACT

The time history of a star of 7 $M_\odot$ undergoing gravitational collapse due to iron decomposition is calculated numerically. The angular velocity assumes a vortexlike distribution which halts the collapse at a relatively low density, 10^{11} g cm^{-3}. The large shear in the velocity field gives an enhancement of about 100 in the multiplication of magnetic-field energy over the energy multiplication from simple compression. The combined effect of rotation and magnetic field is to produce an axial jet. At a radius of 4×10^8 cm where the jet material leaves the calculational grid, the jet carries a mass of 2.1×10^{31} g and a total energy of 1.6×10^{50} ergs. The energy is principally kinetic, 1.6×10^{50} ergs, but it also has a large magnetic energy equal to 3.5×10^{49} ergs, and only 1.1×10^{49} ergs of internal energy.

I. INTRODUCTION

This study was initiated to determine the effect of rotation and magnetic field on the collapse of a star by gravitational instability (Colgate and White 1966; Fowler and Hoyle 1964). The example corresponds to a possible supernova model which depends on the collapse arising from neutrino emission and the thermal decomposition of iron. It is assumed that all material in the star has been completely burned to iron prior to the start of the present calculations. Briefly, the star is started in an equilibrium configuration, and after a few seconds enough energy has been lost by neutrino emission that the star starts to collapse. As this collapse proceeds, the temperature of an interior region rises above the iron-decomposition temperature, and the collapse rapidly accelerates. The rising pressure in the central regions where the iron has been decomposed stops the collapse, and a region of velocity stagnation starts to grow outward from the center of the star. Nonradial motions develop during the collapse due to the increasing centrifugal force. These nonradial motions spread the angular momentum per unit mass evenly over the star, and the angular velocity approaches a vortex configuration. The shear in the velocity generates large magnetic fields along the axis of rotation, and a jet of gas which contains large magnetic fields is expelled from the star along the axis of rotation.

II. MODEL

The numerical calculations are based on a finite-difference representation of hydrodynamic and magnetic equations specialized to axial and equatorial symmetry. The equations are written in cylindrical coordinates R, θ, Z.

The equation for the neutrino energy density ψ is

$$\frac{\partial\psi}{\partial t} + \nabla\cdot(v\psi) = \tfrac{1}{3}c\left[\nabla\cdot\left(\frac{\lambda_t\nabla\psi}{1 + \frac{4}{3}\lambda_t|\nabla\psi/\psi|}\right)\right] + (c/\lambda_c)(aT^4 - \psi) + \left(\psi\frac{\partial\rho}{\partial t}\right)\Big/(3\rho)\,,$$

where ρ, T, and v are the material density, temperature, and velocity, and λ_c, λ_t are the coupling and transport mean free paths for the neutrinos.

The term $1 + \frac{4}{3}\lambda_t\,|\nabla\psi/\psi|$ in the transport term of this equation serves to limit the maximum transport velocity of the neutrinos.

* This work was performed under the auspices of the U.S. Atomic Energy Commission.

The gravitational potential is determined by the solution of the equation

$$\nabla^2\phi = 4\pi G\rho \, .$$

This equation is solved over our finite grid with the boundary values fixed by the field produced at the boundary by the first and third moments of the mass distribution which is interior to the grid. The second mass moment is zero by the symmetry of our problem.

It is assumed that the material is a perfect electrical conductor; therefore, the magnetic equations for field $\boldsymbol{H}$ and current $\boldsymbol{J}$ are

$$\frac{\partial \boldsymbol{H}}{\partial t} = \nabla \times (\boldsymbol{v} \times \boldsymbol{H}) \, , \qquad \nabla \cdot \boldsymbol{H} = 0 \, , \qquad \boldsymbol{J} = (\nabla \times \boldsymbol{H})/4\pi \, .$$

The momentum equation is

$$\rho\left(\frac{\partial \boldsymbol{v}}{\partial t} + \boldsymbol{v}\cdot\nabla\boldsymbol{v}\right) = -\rho\nabla\phi - \nabla\left(P + \frac{\psi}{3 + 4\lambda_t|\Delta\psi/\psi|}\right) + \boldsymbol{J} \times \boldsymbol{H} \, .$$

The equation for density is

$$\frac{\partial \rho}{\partial t} + \nabla\cdot(\rho \boldsymbol{v}) = 0 \, .$$

The equation for material energy E is

$$\frac{\partial(\rho E)}{\partial t} + \nabla\cdot(\boldsymbol{v}\rho E) = -P\nabla\cdot\boldsymbol{v} - (c/\lambda_c)(aT^4 - \psi) \, .$$

The pressure is given by the following set of equations:

$$P = P_{\text{W-H}} + P_T + P_{\text{rad}} \, ,$$

where $P_{\text{W-H}}$ is the material pressure at zero temperature. The fitted equations given by Harrison *et al.* (1965) are used to calculate $P_{\text{W-H}}$. P_T is the electron-baryon pressure due to temperature and is given by:

$$P_T = 1.7 \times 10^{13}\rho NT \, , \qquad N = AZ(1 + 26Z) + 56(1 - AZ)(1 + Z) \, ,$$

$$Z = 1 - \exp\left(-\frac{T + 8888}{2.58\rho^{1/3}Z^{1/3}[A + 11(A + 1)]}\right) ,$$

$$A = 1 + [1 - \sqrt{(1 + 2\beta)}]/\beta \, ,$$

$$\beta = \rho \exp{(8888/T)}/(4.85 \times 10^5 T^{3/2}) \, .$$

The units are cgs except for T, which is in keV. In these equations, Z may be thought of as the number of electrons per baryon and A as the fraction of baryons in iron nuclei.

$$P_{\text{rad}} = 4.57 \times 10^{13}T^4[1 + \tfrac{7}{4}\exp{(-510/T)}] \, .$$

The thermal energies associated with P_T and P_{rad} are

$$E_T = 2.56 \times 10^3[NT + 1280(1 - A)] \, ,$$

$$E_{\text{rad}} = 1.37 \times 10^{14}T^4[1 + \tfrac{7}{4}(1 + 170/T)\exp{(-510/T)}]/\rho \, .$$

Figure 1 shows the isotherms of this equation of state. The mean free paths of neutrinos are given by

$$\lambda_t = 1.6 \times 10^{24}/\rho T^2 , \quad \lambda_c = 1.0 \times 10^{24}/\rho T^2 .$$

The neutrino mean free paths were determined by estimating the rates of neutrino emission from the processes

$$P + \bar{\nu} \leftrightarrow n + e^+ , \quad P + e^- \leftrightarrow n + \nu , \quad e^{\mp} + \nu \leftrightarrow e^{\mp *} + \nu^* \text{ (scattering)} ,$$

$$\nu + \bar{\nu} \leftrightarrow e^+ + e^- ,$$

and plasma neutrinos in the temperature range 1–10 MeV at the appropriate densities. Then a $1/\rho T^2$ variation was assumed, and the constant was adjusted to give a best fit to the rates of energy loss. This mean free path is inaccurate for low temperatures, but at low temperatures the dynamical effects of neutrinos are presumed to be small.

The difference equations are formed with respect to a moving Eulerian grid of 1600 spatial zones (40 zones in each direction). The grid is moved in such a manner as to minimize motion of material relative to the grid. Because the grid is rectangular, a small

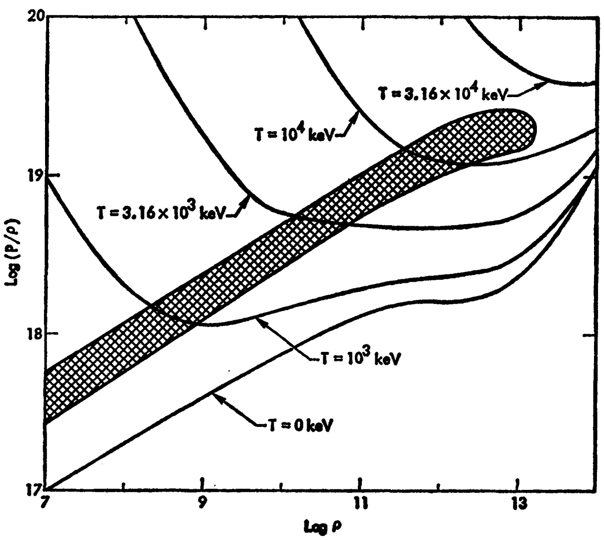

FIG. 1.—Equation-of-state isotherms. Crosshatching indicates the pressure-density regions passed through during the calculation.

density of 10^5 g cm^{-3} has to be placed around the star. The magnetic-field boundary condition is set up to represent vacuum outside the grid.

III. INITIAL CONDITIONS

For an example, a star of 7 $M_{\odot}$ was chosen. Initially, the star was set in a static equilibrium configuration with a central density of 1.2×10^8 g cm^{-3}. Figure 2 shows ρ as a function of T for the central 90 percent of the star's mass. At this density, the central adiabatic γ is just $\frac{4}{3}$, and with a very small neutrino emission the implosion is able to start in a few seconds.

Three configurations were calculated. First, a purely spherical star was followed through its collapse in order to have a standard to gauge the effects of rotation. Second, a star with an initial uniform angular velocity of 0.7 radian sec^{-5} was calculated. This angular velocity corresponds to a kinetic energy of rotation of 0.25 percent of the gravitational energy and a total angular momentum of 4.6×10^{50} g cm^{-2} sec^{-1}. The third calculation had the same angular velocity as the second and, in addition, a polar magnetic field (see Appendix A) whose energy was 0.025 percent of the gravitational energy.

IV. RESULTS OF SPHERICAL CALCULATION

In the spherical nonrotating model, the star begins a rapid collapse after 2.2 sec which is halted at about 2.8 sec by the pressure in the central region becoming high enough to support the star against gravity. The central density at 3 sec is 10^{13} g cm^{-2}. An outward shock is produced, but it has insufficient intensity to blow any material out of the grid. In Figure 3 the gravitational, kinetic, and emitted (radiated) neutrino energies are given as a function of time. The kinetic energy is seen to damp out rapidly, and the star settles back into a slow collapse by neutrino emission.

V. RESULTS OF THE CALCULATION FOR A ROTATING SYSTEM

In this calculation, the early behavior of the collapse is very similar to that of the spherical calculation. However, when the central density rises to about 10^{10} g cm^{-3}, the centrifugal forces become appreciable and the motion becomes appreciably nonradial.

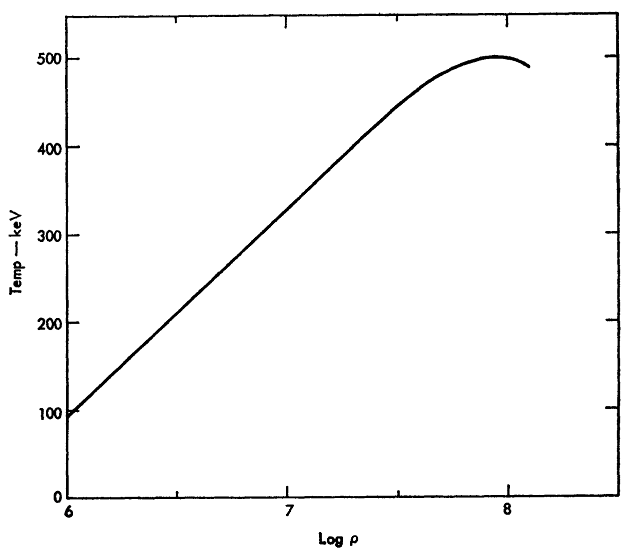

FIG. 2.—Temperature as a function of density at zero time

Collapse is halted at a central density of about 10^{13} g cm^{-3}. The effect of rotation is enhanced by the nonradial motion in the R- and Z-directions which carries angular momentum from regions where it is high to regions where it is low. The angular-velocity distribution gradually approaches a vortex configuration. After 3.5 sec, the distribution of angular velocity, Ω, can be fitted with a power law: $\Omega = 1.6 \times 10^{15}/R^{1.85}$. The exponent of R is either variable or uncertain by about 10 percent. Most of the time the maximum of Ω is at the first zone above the axis, which has a size of 3×10^6 cm. The zoning is not fine enough to determine the nature of the apparent vortex singularity at the axis. A little material is ejected from the grid, but its energy is less than escape energy. In Figure 4, the gravitational energy, kinetic energy in the R- and Z-directions, rotational kinetic energy, and energy emitted in neutrinos are plotted as a function of time. It should be noted that the kinetic energy of rotation is higher than that arising from a simple radial contraction of the star, and, hence, the effect of rotation on impeding the collapse is much greater than it would be for uniform rotation.

VI. RESULTS OF THE CALCULATION FOR A ROTATING MAGNETIZED STAR

As in the calculation for the rotating star, a vortex on the axis and a toroidal swirl near the center are produced during the collapse. The toroidal swirl curls up the field lines

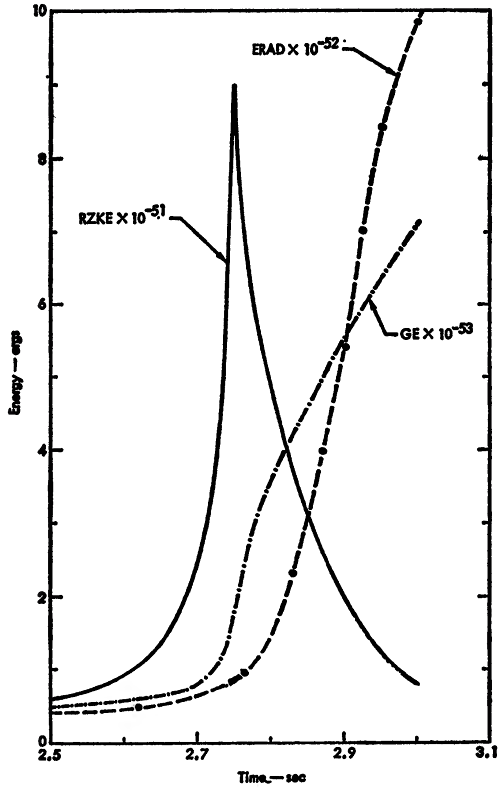

FIG. 3.—Energies as a function of time for spherical calculation. GE = gravitational energy, RZKE = kinetic energy in motions in the R- and Z-directions; and ERAD = energy radiated out of the star.

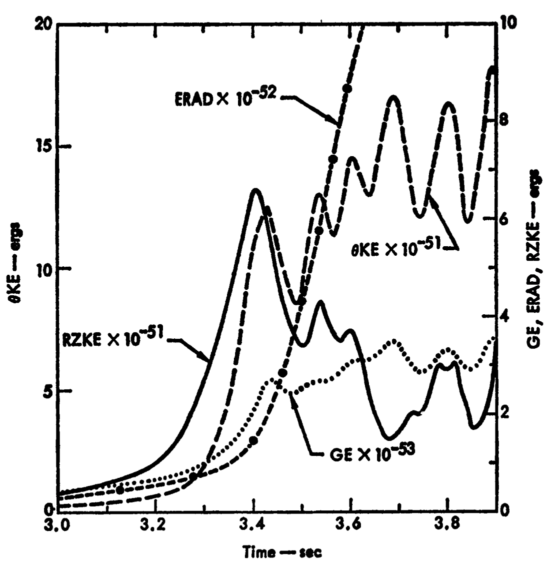

FIG. 4.—Energies as a function of time for rotating calculation. GE = gravitational energy; RZKE = kinetic energy in motions in the R- and Z-directions; ERAD = energy radiated out of the star; and θKE = kinetic energy of rotation about the Z-axis.

and produces high fields (10^{13}–10^{15} gauss). These high fields are thought to be the source of the axial jet which forms shortly after the initial collapse ceases. The magnetic-field energy has risen from 0.025 percent of the gravitational energy to 2.5 percent. Simple contraction of a spherical system leaves the ratio of magnetic energy to gravitational energy unchanged. Thus, the large shearing motions produce an additional factor of 100 in the field generation. Figure 5 shows the (R, Z)-shear,

$$\int \left| \frac{\partial V_Z}{\partial R} - \frac{\partial V_R}{\partial Z} \right| dt \,,$$

integrated over the time interval 2.5–2.65 seconds. From this and from Figure A3*b* it can be seen that the bulk of the star is twisted up several revolutions during the tenth

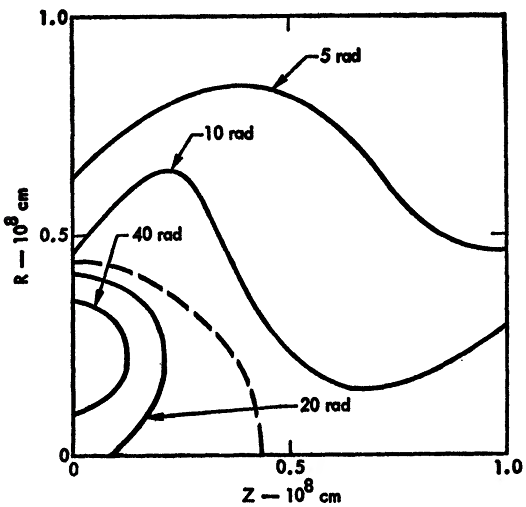

Fig 5

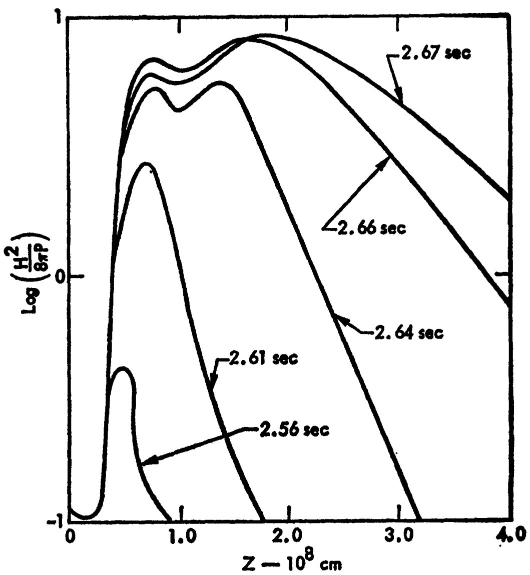

Fig. 6

Fig. 5.—Contours of shear in the (R, Z)-plane integrated from 2.5 to 2.65 sec. Dashed curve contains within it one-half of the stellar mass.

Fig. 6.—Ratio of magnetic-field energy density to material pressure along the axis.

of a second when the jet starts. In Figure 6 we see the buildup of the ratio of magnetic-field pressure to material pressure near the axis. The high-field region at about $Z = 7 \times 10^7$ cm is probably the origin of the jet.

The axial jet at the end of the calculation had ejected 2.1×10^{31} g of material with a kinetic energy of 1.6×10^{50} ergs, a thermal energy of 1.1×10^{49} ergs, a magnetic energy of 3.5×10^{49} ergs, and a gravitational energy of -4.7×10^{49} ergs (see Fig. 7 for rates of flow in the jet). Figure 8 includes the curves for the same energies as Figure 4, plus the magnetic energy as a function of time. Typical temperatures, densities, and magnetic fields in the jet are, respectively, 300 keV, 10^6 g cm^{-3}, and 10^{13} gauss.

VII. DISCUSSION OF RESULTS

The spherical problem is of interest in that it is an example of gravitational collapse by iron decomposition from which no material is ejected (cf. Colgate and White 1966; Schwartz 1967; Arnett 1966).

The vortex motion produced in the rotating collapse is the most important feature of the effect of rotation. The axial symmetry of the calculation forces any convective mo-

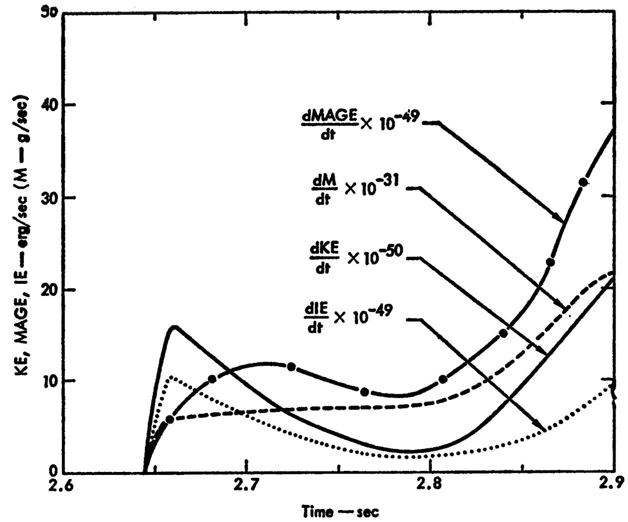

FIG. 7.—Rate of emission of mass and energies by the axial jet. KE = kinetic energy; MAGE = energy in magnetic field; IE = internal energy; and M = mass.

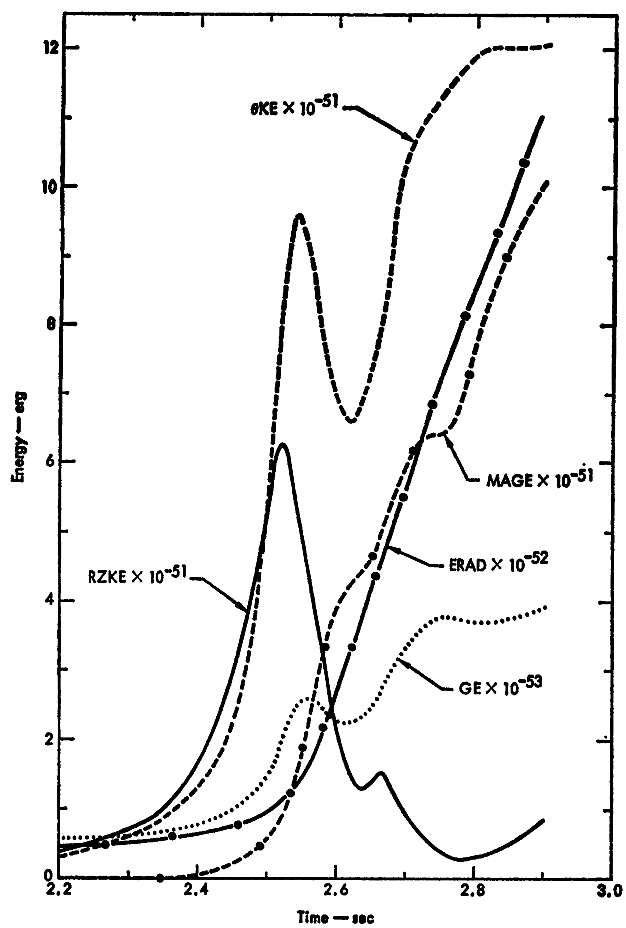

FIG. 8.—Energies as a function of time for magnetized-star calculation. GE = gravitational energy; RZKE = kinetic energy in motions in the R- and Z-directions; ERAD = energy radiated out of the star; θKE = kinetic energy of rotation about the Z-axis; and MAGE = energy in magnetic field.

tions to be of such a nature as to smooth out the angular momentum (Bretherton and Turner 1968). In a real three-dimensional world it is not clear how long it would take for an isotropically turbulent condition to set in, but it should take a few sound-transit times. Hence, we expect the behavior in a real system to follow these calculations for early times, but at late times the calculations probably overestimate the large-scale order in the spatial distribution of the velocity.

Due to the excessive computer time required to complete the calculations, the following crude method was used to estimate the total amount of material and energy that might eventually be ejected by the jet. It is presumed that the primary mechanism of the expulsion is the generation of a large magnetic field in a limited region so that the material becomes buoyant and rises as a bubble. The rotational motion is distributed as $\Omega \sim 1/R^2$, which implies a great deal more rotational energy than would arise for a constant angular-velocity distribution. We shall assume that all the rotational kinetic energy is available to produce the magnetic field. The magnetic field is generated near the center of the star at a low gravitational potential. The magnetic field energy per gram is estimated by taking the ratio of the total energy in the jet to mass in the jet at the surface and multiplying it by the ratio of the surface radius R to the mean radius $\langle R \rangle$ defined by the equation (gravitational energy $= GM^2/\langle R \rangle$). The following values are found: $\langle R \rangle = 3.25 \times 10^7$ cm, $R_{\text{surface}} = 3.5 \times 10^8$ cm. Total energy per gram in the jet at the surface $= 1.0 \times 10^{19}$ ergs g^{-1}. Hence, the energy extrapolated to the $\langle R \rangle$ is 1.0×10^{20} ergs. Since a rotational energy of 1.2×10^{52} ergs is available, we estimate a total emitted jet mass equal to 1.2×10^{32} g, which carries 1.2×10^{51} ergs of energy.

Although these numbers could explain some supernova observations, the authors have seen no pictures of supernova remnants suggestive of jets. This, of course, could be due to the dispersion of the jet by a surrounding envelope. It is not clear from our calculations what the history of the remaining material in the star would be. However, the star has retained a mass large enough so that it is unstable against further collapse.

Perhaps of more interest is the bearing these calculations may have on the jets observed in radio galaxies. The analogous picture for a galaxy would be for the galaxy to form out of an initially slowly rotating, weakly magnetized blob of gas that undergoes considerable free fall and then is halted by some mechanism.

One of the authors (J. R. W.) would like to thank D. Sciama and the Department of Applied Mathematics and Theoretical Physics, University of Cambridge, for their hospitality while part of this work was done. We would also like to thank Mr. J. Chase, who did much of the program development.

APPENDIX A

SPATIAL-CONFIGURATION GRAPHS

Figure A1 gives the initial configurations of density and magnetic field. Figures A2*a*, A2*b*, A3*a*, and A3*b* show, respectively, the density, the magnetic-field flux parallel to the Z-axis, the intensity of the θ-component of magnetic field, and the angular velocity at a time of 2.67 sec, which is shortly after the jet has emerged to the surface. Figures A4–A6 show the velocity vectors associated with each grid point at several different times from the start of bounce through the formation of the jet.

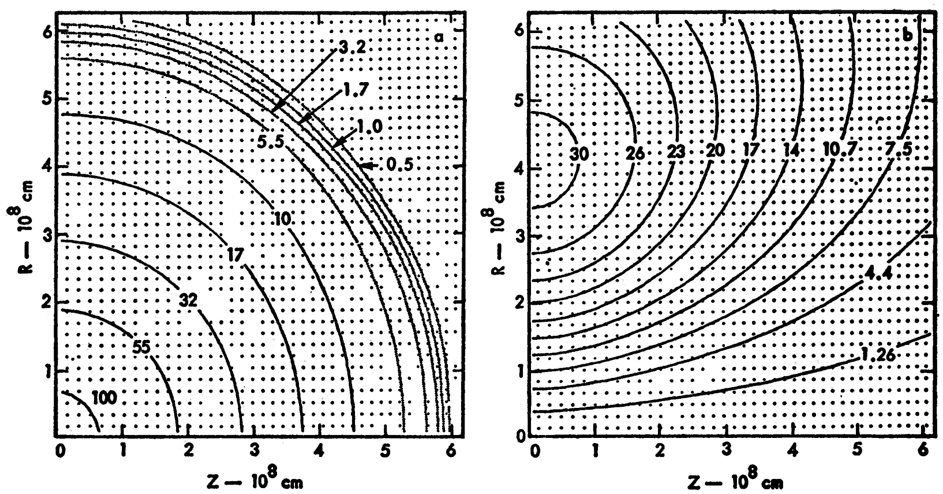

FIG. A1*a*.—Isodensity contours in units of 10^6 g cm^{-3} at 0.72 sec.
FIG. A1*b*.—Magnetic-flux contours parallel to Z-axis in units of 10^{22} gauss cm^{-2} at 0.72 sec.

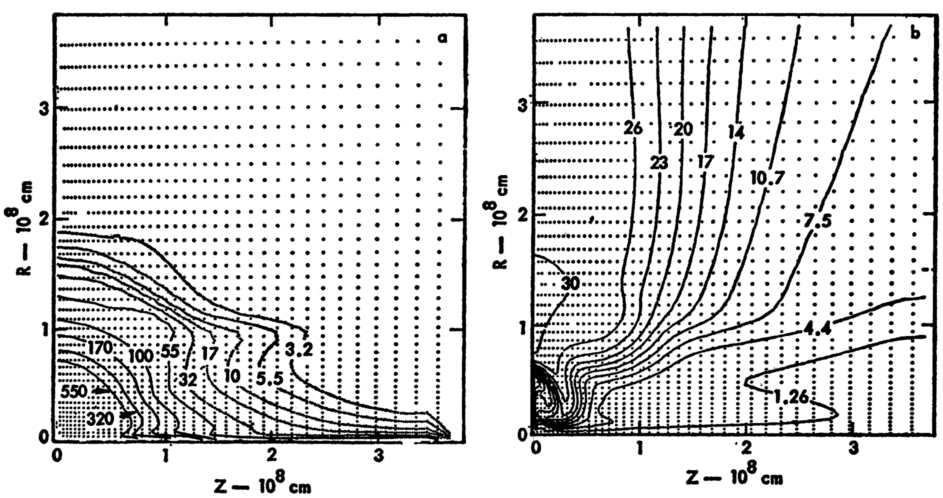

FIG. A2*a*.—Isodensity contours in units of 10^6 g cm^{-3} at 2.67 sec.
FIG. A2*b*.—Magnetic-flux contours parallel to Z-axis in units of 10^{22} gauss cm^{-2} at 2.67 sec.

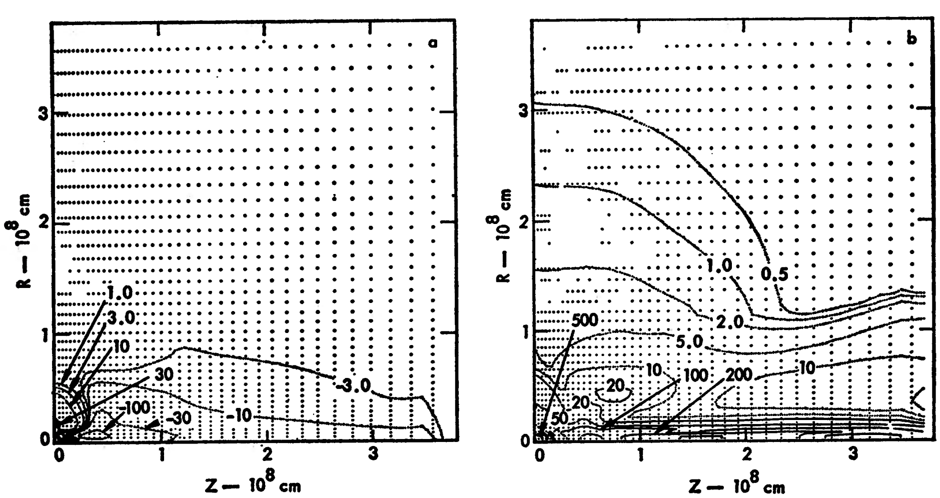

FIG. A3*a*.—Theta magnetic-field contours in units of 10^{13} gauss at 2.67 sec.
FIG. A3*b*.—Iso–angular-velocity contours in radians per second at 2.67 sec.

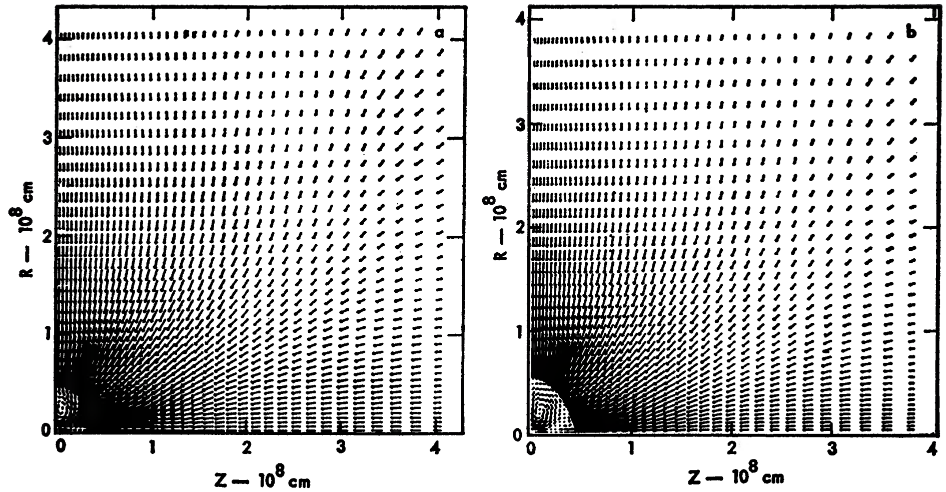

FIG. A4*a*.—Velocity-vector plot at 2.52 sec. Maximum velocity magnitude = 2.42×10^9 cm sec^{-1}. (For all velocity plots, the length of the maximum velocity vector is one-twentieth the figure size.)
FIG. A4*b*.—Velocity-vector plot at 2.56 sec. Maximum velocity magnitude = 3.05×10^9 cm sec^{-1}.

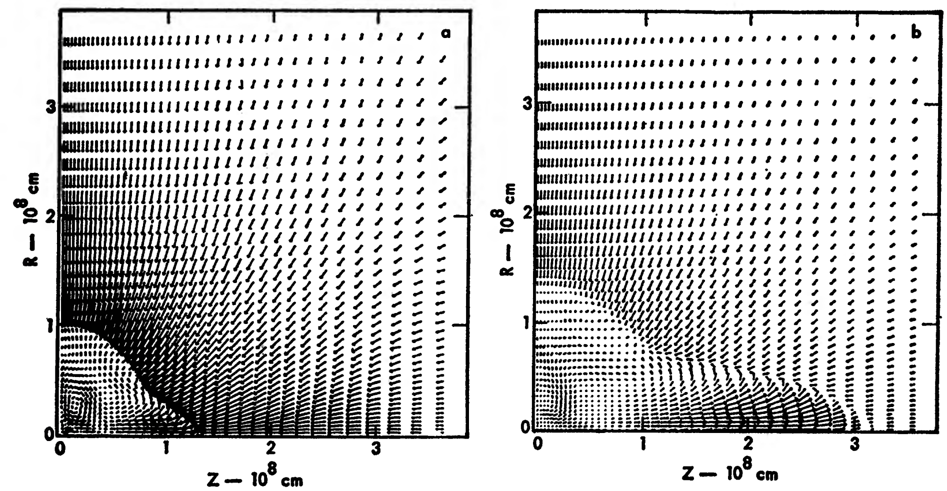

FIG. A5*a*.—Velocity-vector plot at 2.61 sec. Maximum velocity magnitude = 2.43×10^9 cm sec^{-1}.
FIG. A5*b*.—Velocity-vector plot at 2.64 sec. Maximum velocity magnitude = 4.38×10^9 cm sec^{-1}.

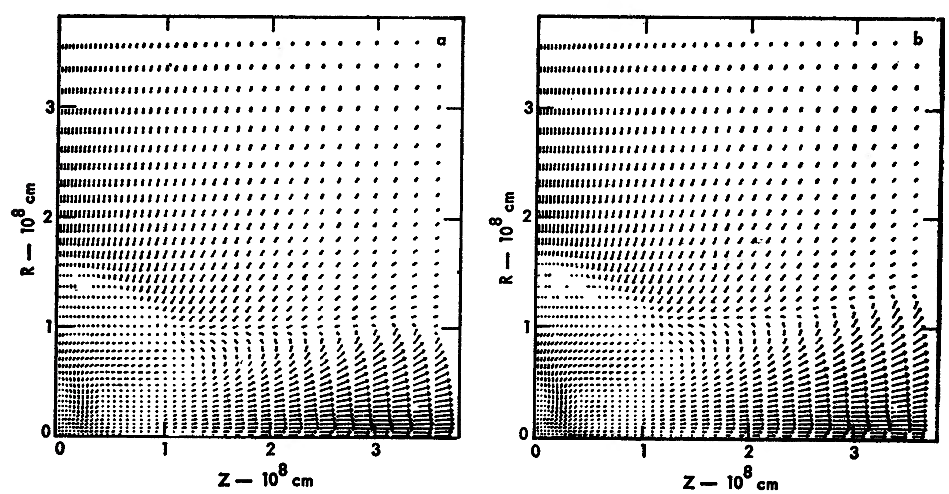

FIG. A6*a*.—Velocity-vector plot at 2.66 sec. Maximum velocity magnitude = 6.04×10^9 cm sec^{-1}.
FIG. A6*b*.—Velocity-vector plot at 2.67 sec. Maximum velocity magnitude = 5.60×10^9 cm sec^{-1}.

APPENDIX B

NUMERICAL ENHANCEMENT OF VORTEX MOTION

The possibility is present that some of the formation of vortex motion along the axis is generated by differencing errors. We may write the equation for angular-momentum density A about the symmetry axis in a mixing-length approximation as

$$\frac{\partial A}{\partial t} + \nabla \cdot (AV) = \nabla \cdot (l\boldsymbol{v}\nabla A) + \nabla \cdot (\eta_c \nabla A) ,$$

where V is the gross (overall) velocity, $\boldsymbol{v}$ is the velocity associated with a small swirl of size l, and η_c is the artificial viscosity introduced by finite differencing. This viscosity is approximated by $\eta_c = \Delta R \Delta V$, where ΔR is the zone size and ΔV is the velocity across the zone. We can relate η_c to $l\boldsymbol{v}$ by $\eta_c \approx l\boldsymbol{v}/n^2$, where n is the mean number of zones in a swirl. Most of the velocity gradients involve at least five or ten zones (see Figs. A4–A6), and so the errors should be only a few percent. The errors incurred during the main collapse are a little harder to estimate. The grid system of the difference equations was moved during the collapse in such a way as to minimize the net flow with respect to the grid; however, some relative flow is left which adds to the differencing errors.

REFERENCES

Arnett, W. D. 1966, *Canadian J. Phys.*, **44**, 2553.
Bretherton, F. P., and Turner, J. S. 1968, *J. Fluid Mech.*, **32**, 449.
Colgate, S. A., and White, R. H. 1966, *Ap. J.*, **143**, 626.
Fowler, W. A., and Hoyle, F. 1964, *Nucleosynthesis in Massive Stars and Supernovae* (Chicago: University of Chicago Press).
Harrison, B. K., Thorne, K. S., Wakano, M., and Wheeler, J. A. 1965, *Gravitational Theory and Gravitational Collapse* (Chicago: University of Chicago Press).
Schwartz, R. A. 1967, *Ann. Phys.*, **43**, 42.